Received: 17 July 2023 | Revised: 19 September 2023 | Accepted: 3 October 2023

DOI: 10.1002/mp.16787

RESEARCH ARTICLE

MEDICAL PHYSICS

Quantitative analysis of aortic Na[^{18}F]F uptake in macrocalcifications and microcalcifications in PET/CT scans

Gijs D. van Praagh[1] | **Mirjam E. J. Davidse**[2] | **Jelmer M. Wolterink**[2] | **Riemer H. J. A. Slart**[1,3]

[1]Department of Nuclear Medicine & Molecular Imaging, Medical Imaging Center, University of Groningen, University Medical Center Groningen, Groningen, The Netherlands

[2]Department of Applied Mathematics and Technical Medicine Center, University of Twente, Enschede, The Netherlands

[3]Department of Biomedical Photonic Imaging, University of Twente, Enschede, The Netherlands

Correspondence
Gijs D. van Praagh, Department of Nuclear Medicine and Molecular Imaging, Medical Imaging Center, University Medical Center Groningen, Hanzeplein 1, 9713 GZ, Groningen, The Netherlands.
Email: g.d.van.praagh@umcg.nl

Abstract

Background: Currently, computed tomography (CT) is used for risk profiling of (asymptomatic) individuals by calculating coronary artery calcium scores. Although this score is a strong predictor of major adverse cardiovascular events, this method has limitations. Sodium [^{18}F]fluoride (Na[^{18}F]F) positron emission tomography (PET) has shown promise as an early marker for atherosclerotic progression. However, evidence on Na[^{18}F]F as a marker for high-risk plaques is limited, particularly on its presentation in clinical PET/CT. Besides, the relationship between microcalcifications visualized by Na[^{18}F]F PET and macrocalcifications detectable on CT is unknown.

Purpose: To establish a match/mismatch score in the aorta between macrocalcified plaque content on CT and microcalcification Na[^{18}F]F PET uptake.

Methods: Na[^{18}F]F-PET/CT scans acquired in our centre in 2019–2020 were retrospectively collected. The aorta of each low-dose CT was manually segmented. Background measurements were placed in the superior vena cava. The vertebrae were automatically segmented using an open-source convolutional neural network, dilated with 10 mm, and subtracted from the aortic mask. Per patient, calcium and Na[^{18}F]F-hotspot masks were retrieved using an in-house developed algorithm. Three match/mismatch analyses were performed: a population analysis, a per slice analysis, and an overlap score. To generate a population image of calcium and Na[^{18}F]F hotspot distribution, all aortic masks were aligned. Then, a heatmap of calcium HU and Na[^{18}F]F-uptake on the surface was obtained by outward projection of HU and uptake values from the centerline. In each slice of the aortic wall of each patient, the calcium mass score and target-to-bloodpool ratios (TBR) were calculated within the calcium masks, in the aortic wall except the calcium masks, and in the aortic wall in slices without calcium. For the overlap score, three volumes were identified in the calcium and Na[^{18}F]F masks: volume of PET (PET+/CT-), volume of CT (PET-/CT+), and overlapping volumes (PET+/CT+). A Spearman's correlation analysis with Bonferroni correction was performed on the population image, assessing the correlation between all HU and Na[^{18}F]F vertex values. In the

Abbreviations: Asc, ascending aorta; CT, computed tomography; DSC, dice similarity coefficient; HU, Hounsfield unit; MACE, major adverse cardiovascular events; Na[^{18}F]F, sodium [^{18}F]fluoride; PET, positron emission tomography; SVC, superior vena cava; TBR, target-to-background ratio; VOI, volume of interest.

per slice analysis, a paired Wilcoxon signed-rank test was used to compare TBR values within each slice, while an ANOVA with post-hoc Kruskal–Wallis test was employed to compare TBR values between slices. p-values < 0.05 were considered significant.

Results: In total, 186 Na[^{18}F]F-PET/CT scans were included. A moderate positive exponential correlation was observed between total aortic calcium mass and total aortic TBR ($r = 0.68, p < 0.001$). A strong positive correlation ($r = 0.77$, $p < 0.0001$) was observed between CT values and Na[^{18}F]F values on the population image. Significantly higher TBR values were found outside calcium masks than inside calcium masks ($p < 0.0001$). TBR values in slices where no calcium was present, were significantly lower compared with outside calcium and inside calcium (both $p < 0.0001$). On average, only 3.7% of the mask volumes were overlapping.

Conclusions: Na[^{18}F]F-uptake in the aorta behaves similarly to macrocalcification detectable on CT. Na[^{18}F]F-uptake values are also moderately correlated to calcium mass scores (match). Higher uptake values were found just outside macrocalcification masks instead of inside the macrocalcification masks (mismatch). Also, only a small percentage of the Na[^{18}F]F-uptake volumes overlapped with the calcium volumes (mismatch).

KEYWORDS
analysis, aorta, atherosclerosis, calcium, match/mismatch, Na[^{18}F]F, positron emission tomography computed tomography

1 | INTRODUCTION

Major adverse cardiovascular events (MACE), such as stroke and heart attack, remain leading global causes of death.[1] Currently, computed tomography (CT) is used for risk profiling of (asymptomatic) individuals by calculating coronary artery calcium scores. This score is a well-known and strong predictor of MACE, even more so is a zero calcium score a proven strong negative predictor.[2,3] However, this method has limitations. Calcium scores, that is, the Agatston score or the more stable calcium mass score, increase with higher volume and higher density calcifications, while microcalcifications (~5–60 μm) and low-density calcifications play an important role in plaque rupture.[4–10] These microcalcifications have a size smaller than the spatial resolution of state-of-the-art CT scanners.[11–14] On the other hand, extended calcifications visible on CT stabilize and are less prone to rupture.[6,15,16] Moreover, while calcium scores increase with lesion density, lower-density calcifications are associated with a higher risk for MACE.[9,17] Additionally, non-observed calcifications in patients that appear to have a zero calcium score on CT have been shown to have a higher risk.[18] Progression of calcifications is a slow process, taking months or years to be visible on CT, which makes CT a suboptimal method to capture these high-risk vulnerable plaques.

An increasing number of studies have demonstrated the potential of sodium [^{18}F]fluoride (Na[^{18}F]F) positron emission tomography (PET) combined with CT as an early marker for atherosclerotic progression.[16,19,20] Na[^{18}F]F is currently clinically used as a bone tracer and is shown to bind to ongoing mineralization.[21] It is highly specific to the surface of actively progressive calcifications. As microcalcifications have relatively more surface area than macrocalcifications detected by CT, Na[^{18}F]F is hypothesized to visualize microcalcifications of high-risk plaques.

However, evidence on Na[^{18}F]F as a marker for high-risk plaques is limited, particularly on its presentation in clinical PET/CT. Besides, the relationship between microcalcifications visualized by Na[^{18}F]F PET and macrocalcifications detectable on CT is unknown. As the resolution of PET/CT is suboptimal for small areas and vascular Na[^{18}F]F uptake is substantially lower than in bones, it is challenging to evaluate these processes. Moreover, most studies focused on Na[^{18}F]F uptake in coronary arteries, whereas the better visible aorta on PET/CT is less studied.[19,20] Therefore, this study aims to establish a match/mismatch score in the aorta between macrocalcified plaque content on CT and microcalcification Na[^{18}F]F PET uptake.

2 | METHODS AND MATERIALS

2.1 | Patient data and scan acquisition

Data and PET/CT scans of all patients who underwent a total body Na[^{18}F]F-PET/CT at the University Medical Center Groningen between January 2019 and December 2020 were retrospectively collected from the electronic patient file system and the picture archive and commication system. All patients underwent this scan

TABLE 1 Patient characteristics and scanner acquisition and reconstruction settings.

Characteristics	*N* (%) or mean ± SD or median (IQR)
No. of patients	186
Age on date of scan (years) [range]	60.5 ± 17.6 [7.0–92.0]
Sex-type (males)	101 (54%)
BMI (kg/m2) [range]	23.16 ± 9.5 [15.1–43.2][a]
Scanners	
Biograph mCT40	53 (28%)
Biograph mCT64	64 (34%)
Biograph vision	70 (37%)
Tube voltage (kV)	80 (*N* = 3), 100 (*N* = 13), 120 (*N* = 144), 140 (*N* = 27)
Tube current time product (mAs)	11.5 (8.5–18.5)
Slice thickness (mm)	3
Matrix size (pixel × pixel)	512 × 512

Abbreviations: BMI, body mass index; IQR, interquartile range; SD, standard deviation.
[a]Of 21 patients, length and/or weight was unknown.

for suspection of bone metastases, due to breast or prostate cancer. Follow-up scans were removed from the analysis. Because of its retrospective nature, the Medical Research Involving Human Subjects Acts (WMO) obligation was waived by the local ethics committee. Therefore, the objection registry was checked for all patients, but informed consent was not obtained. Data was stored and processed pseudonymized.

Scans were acquired on one of three scanners (Biograph mCT40, Biograph mCT64, or Biograph Vision, Siemens Healthineers, Knoxville, TN, USA). See Table 1 for the patient characteristics and PET/CT scan parameters. Na[18F]F-PET/CTs were performed according to the European Association of Nuclear Medicine procedure guidelines.[22] After at least 6 h of fasting, 2–3 MBq/kg of tracer was intravenously administered to the patient, depending on the used scanner system. Sixty minutes after administration, a low-dose CT and subsequent PET scan from skull to knee, 1–2 min per bed position, were performed.

2.2 | Aorta and vertebrae segmentation

The aorta of every low-dose CT was manually segmented into four regions (ascending aorta, aortic arch, descending aorta, and abdominal aorta) in Affinity Viewer (version 2.0.3; Hermes Medical Solutions, Stockholm, Sweden). The ascending aorta was delineated from the slice just above the aortic valve up to the first aortic branch, the aortic arch from the next slice up to and including the slice past the last aortic branch, the descending aorta from the next slice up to and including the diaphragm, and the abdominal aorta from the next slice up to the iliac bifurcation. Furthermore, background measurements were taken by placing three 1 mL volumes of interest (VOIs) in the superior vena cava (SVC) and three 1 mL VOIs in the center of the ascending aorta (Asc). If cardiovascular devices, like leads, were present in the SVC, thus influencing background measurements, the VOIs were placed in the inferior vena cava.

As Na[18F]F uptake in bones is substantially higher than in vessels, spill-over from the vertebrae into the adjacent aorta needs to be excluded. Therefore, the vertebrae were automatically segmented using an open-source convolutional neural network.[23] After examination, these vertebral segmentation masks were closed and dilated with 10 mm using morphological operations and subtracted from the aortic mask. The rationale for 10 mm dilation is described in the supplementary materials and methods and supplementary results (Figures S1 and S2). From here on, when refered to the aortic mask in this paper, the aortic mask with the dilated vertebral mask subtracted is meant.

2.3 | Calcium and Na[18F]F

Per patient, calcium and Na[18F]F hotspot masks were obtained using an in-house developed algorithm. As a lower threshold for calcium masks we used the mean Hounsfield unit (HU) plus three times the SD from the ascending aortic background measurments as described by Raggi et al.[24]: $calcium\_threshold = HU_{mean}(Asc\ background) + 3 * HU_{SD}(Asc\ background)$. To exclude voxels exceeding the threshold due to imaging noise in the lumen, an artificial aortic wall was created as the outer 5 mm of the aortic mask. As a lower threshold for Na[18F]F hotspots we used the adaptive 50% SUV_{peak} threshold as described by Frings et al.[25] In short, the SUV_{peak} in a sphere with a diameter of 12 mm was measured within the aortic mask. In contrast to Frings et al., we limited the entire sphere instead of only the center voxel to the boundaries of the aortic mask to avoid vertebral uptake. The lower threshold in the full aortic mask was then set to: $NaF\_threshold = SUV_{mean}(SVC\ background) + 0.5 * SUV_{peak}(aorta)$. Using these lower thresholds within the aortic mask, three match/mismatch analyses were performed: a 2D population image, a 2D per slice analysis, and a 3D overlap score.

2.4 | Population image

To generate a population image of calcium and Na[18F]F hotspot distribution, all aortic masks were aligned using SimpleElastix.[26] The volume of the bounding box around each aortic mask was calculated and the mask with the median volume was set as a fixed image. Due to the shape variability of aortas, registration was

performed per aortic segment. Before registration, spacing, direction, and origin of every mask were set to the spacing, direction, and origin of the fixed image. Subsequently, affine registration and b-spline registration were performed. All settings can be found in Table S1. The results were verified by calculating a Dice similarity coefficient (DSC) between the registered mask and the fixed mask. A DSC above 0.8 was considered sufficient. If the DSC was lower than this threshold, masks were manually cropped to ensure the masks would overlap with the fixed mask before registration. The resulting transformation matrix was then used to transform the calcium images and Na[^{18}F]F images. All calcium images and Na[^{18}F]F images were then summed.

A surface mesh and centerline of the median aorta was extracted using marching cubes. Then, a heatmap of calcium HU and Na[^{18}F]F uptake on the aorta surface was obtained by outward projection of HU values and SUV from the centerline.

2.5 | Per slice analysis

In each slice of the aortic wall of each patient, the calcium mass score was calculated and calcium masks were extracted using the previously determined calcium threshold. In addition, on the PET images, target-to-bloodpool ratios (TBR) were calculated within the calcium masks (i.e., "in calcium"), in the aortic wall except the calcium masks (i.e., "outside calcium"), and in the aortic wall in slices without calcium (i.e., "no calcium").

2.6 | Overlap score

Comparing the calcium and Na[^{18}F]F masks, three volumes were identified: volume of PET with no overlap of CT (PET+/CT–), volume of CT with no overlap of PET (PET–/CT+), and volumes with both PET and CT (PET+/CT+). The percentage of each volume present in each patient was calculated.

2.7 | Statistical analysis

Normally distributed data was presented as mean ± SD and non-parametric data as median [interquartile range (IQR)]. First, a Pearson's correlation analysis was done between the total aortic TBR, defined as the total aortic Na[^{18}F]F uptake divided by the background SUV_{mean}. Second, a Spearman's correlation analysis with Bonferroni correction on its p-values was performed on the population image, assessing the correlation between all HU and Na[^{18}F]F vertex values. Then, for every vertex on the surface meshes, a Spearman's correlation analysis with Bonferroni correction on its *p*-values was performed between the HU values of that vertex and its 500 closest vertices and the Na[^{18}F]F values of that vertex and its 500 closest vertices. All vertices that overlapped with the 10 mm dilated vertebra of the median patient were excluded from the correlation analysis. Descriptive analysis was done on the distribution of calcium and Na[^{18}F]F in the population images. In the per slice analysis, a paired Wilcoxon signed-rank test was used to compare TBR values within each slice, while an ANOVA with post-hoc Kruskal-Wallis test was employed to compare TBR values between slices. *p*-values < 0.05 were considered significant. The surface mesh correlation analysis was performed using Python (version 3.9). All other statistical analyses were conducted using GraphPad Prism (version 9.1.0, GraphPad Software Inc., San Diego, CA, USA).

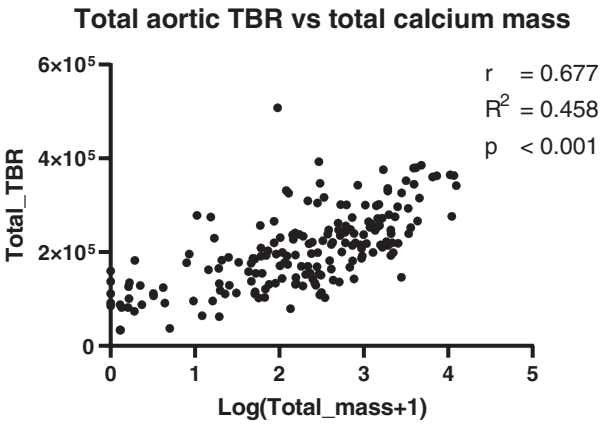

FIGURE 1 Total aortic TBR—defined as total SUV Na[^{18}F]F devided by SUV_{mean} background—plotted against the log of the total aortic calcium mass reveals a moderate exponential correlation. TBR, target-to-background ratio; SUV, standardized uptake value.

3 | RESULTS

In total, 250 Na[^{18}F]F-PET/CT scans were collected; 43 of these were follow-up scans, 11 were incomplete, and 10 were removed as it was impossible to segment the vertebrae due to anatomical abnormalities caused by bone metastases or metal implants. Thus, 186 Na[^{18}F]F-PET/CT scans were used in the analyses.

A moderate positive exponential correlation was observed between total aortic calcium mass and total aortic TBR ($r = 0.68$, $p < 0.001$; Figure 1).

3.1 | Population image

A strong positive correlation ($r = 0.77$, $p < 0.0001$) was observed between all HU and Na[^{18}F]F values on the population image (Figure 2). Figure 3 demonstrates the calcium and Na[^{18}F]F hotspot distribution of the population. The supplementary material provides a video

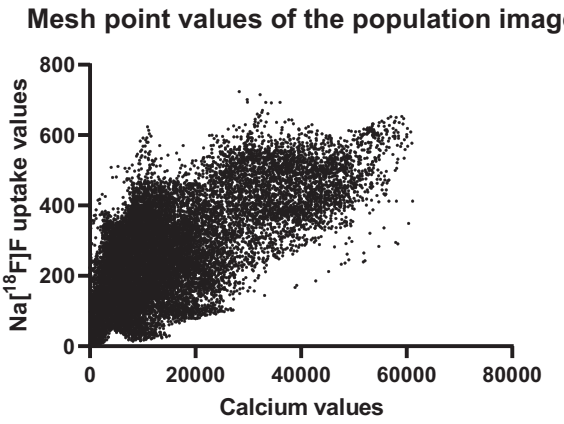

FIGURE 2 All mesh point values of the population image. A clear positive correlation is seen. Also, most points have relatively higher Na[18F]F uptake than calcium values.

showing the complete 3D view of this result (Video S1). Most calcifications in the population were clearly visible in the inferior abdominal aorta and the inferior aortic arch. Most Na[18F]F uptake was observed in similar parts, as well as in the superior abdominal aorta. When inspecting the correlation per location on the mesh, 79% of locations had a positive correlation (63% $p < 0.05$), with 25% above 0.6 (all $p < 0.05$), while 21% had a negative correlation (9% $p < 0.05$) and 0% below −0.6. Around 11% of all mesh points had low calcium and low Na[18F]F uptake (below 10% of the maximum). Video S2 visualizes the corresponding calculated Spearmans' *r* value for each mesh point. Mesh points overlapping with the dilated vertebra of the median patient were excluded from the correlation analysis.

Videos S3 and S4 show videos of these distributions for groups aged under 65 and 65 or older, as well as the distributions of an aged-matched male and female group. The distribution of calcium and Na[18F]F in younger people is similar to the older group, but with lower values. In the anterior superior aortic arch a high amount of Na[18F]F uptake is observed in the younger group, whereas there is little to no uptake in the older group at that location. No large differences in the location of calcium and Na[18F]F were observed between females and males. Slightly larger Na[18F]F hotspots were observed in the abdomen of males compared with females, whereas in the arch and descending aorta hotspots were observed slightly larger in females compared with males.

3.2 | Per slice analysis

TBR values were significantly higher outside the calcium masks compared with inside the calcium masks ($p < 0.0001$). TBR values in slices without calcium were significantly lower compared with those outside calcium and inside calcium (both $p < 0.0001$; Figure 4).

Slices were categorized into six groups based on calcium mass scores: 0–1 mg, 1–5 mg, 5–10 mg, 10–20 mg, 20–50 mg, and 50+ mg. Pairwise analysis showed significantly higher TBR values outside the calcification masks than inside the calcification masks for every group (all $p < 0.0001$), except for the calcifications with 50+ mg ($p = 0.48$; Figure 5).

3.3 | Overlap score

After extracting the 3D volumes of Na[18F]F masks and calcium masks from all patients, little overlap was observed between the masks. On average only 3.7% of the volumes overlapped. PET+/CT- masks comprised on average 66.8% of the volumes and PET-/CT+ masks comprised on average 29.5% (Figure 6). In the group of patients with a total calcium mass score lower than 215 mg (median mass score of the population) the average volumes of PET+/CT-, PET-/CT+, and PET+/CT+, were 76.0%, 23.0%, and 1.0%, respectively. In the group of patients with a total calcium mass score higher than 215 mg the average volumes of PET+/CT-, PET-/CT+, and PET+/CT+ were 58.1%, 35.8%, and 6.1%, respectively.

4 | DISCUSSION

In this study, we found a moderate correlation (match) between total aortic Na[18F]F uptake and aortic calcium mass. Additionally, a strong correlation (high match) was observed between the location of detectable macrocalcifications on low-dose CT and Na[18F]F uptake. Conversely, we found a mismatch in uptake with significantly higher TBR values outside the macrocalcifications compared with inside the macrocalcifications. Moreover, only a small percentage of the Na[18F]F uptake volumes overlapped with the calcium volumes.

Na[18F]F-PET/CT is used clinically to detect metastases in bone, breast, and prostate cancer. Growing evidence suggests the potential of Na[18F]F as an early marker for plaque vulnerability and future cardiovascular risk.[19,20] Preclinical studies demonstrated high specificity of Na[18F]F for vascular calcifications, more specifically their surface.[16,27] Smaller calcifications have relatively more surface, theoretically resulting in relatively more Na[18F]F uptake. Small prospective clinical trials have also demonstrated its potential as risk stratification for cardiovascular disease.[19,27] However, evidence is limited, especially on its presentation in clinical PET/CT.

Den Harder et al. reported a weak correlation between TBR and calcium mass.[28] In our study, we found a moderate exponential correlation between total aortic TBR

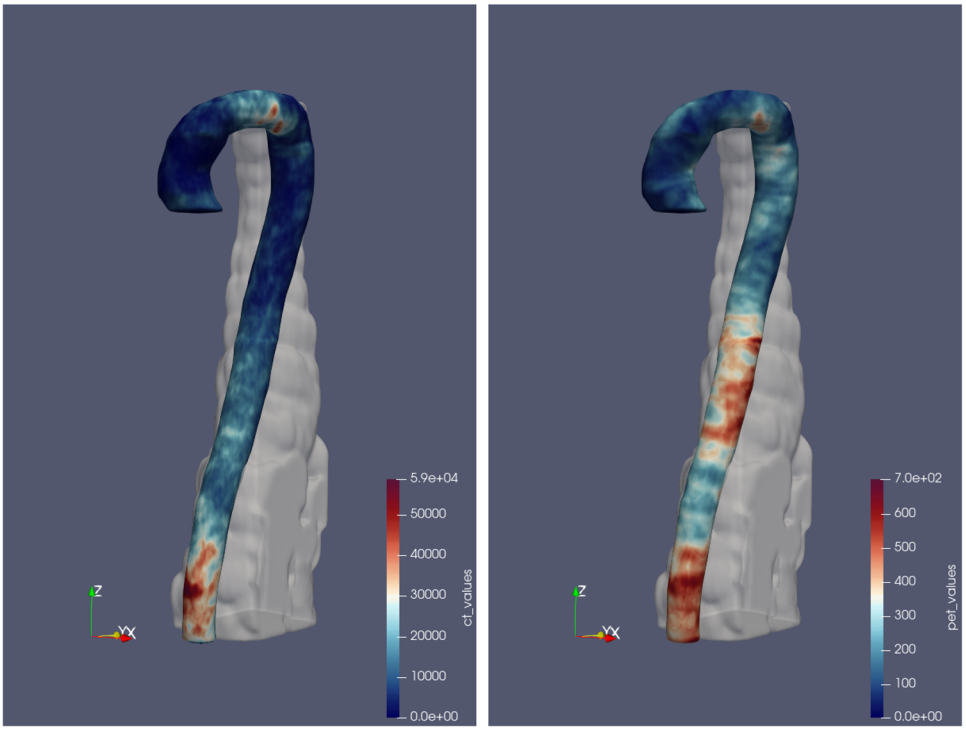

FIGURE 3 Calcium distribution on CT (left) and Na[^{18}F]F distribution (right) of the entire population. In transparent white, the dilated vertebral mask of the "median patient" is shown.

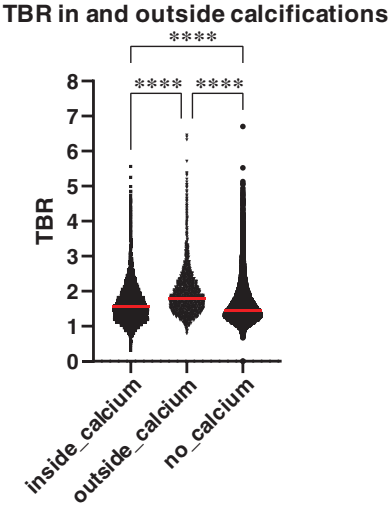

FIGURE 4 In every slice of every patient, target-to-bloodpool ratio (TBR) calculated inside calcium masks, in the aortic wall outside calcium masks and the aortic wall in slices where no calcium was present. In order from high to low, significantly higher TBR values were found outside calcifications than inside calcifications and in slices without calcifications.

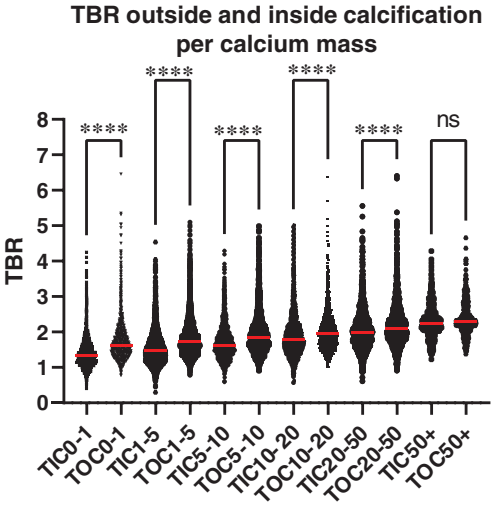

FIGURE 5 Calcification mass per slice was separated into six groups: mass score 0–1, 1–5, 5–10, 10–20, 20–50, and 50+ mg. Target-to-bloodpool ratios (TBR) were calculated inside the calcification masks (TIC), and outside the calcification masks within the same slice (TOC). A pairwise analysis showed significantly higher TBR values outside the calcification masks than inside the calcification masks for every group, except for the calcifications with 50+ mg.

and total aortic calcium mass. The results are difficult to compare as it is not clear whether the calcium mass used in the study of den Harder et al. is per slice, per vessel, or per patient, and units are missing. We used the natural logarithm of total calcium mass, which might cause the difference. Besides, we measured in the aorta whereas den Harder et al. focused on the femoral arteries. Atherosclerosis is—despite its systemic nature and similar pathogenetic mechanisms—a disease with different faces. The morphological characteristics of

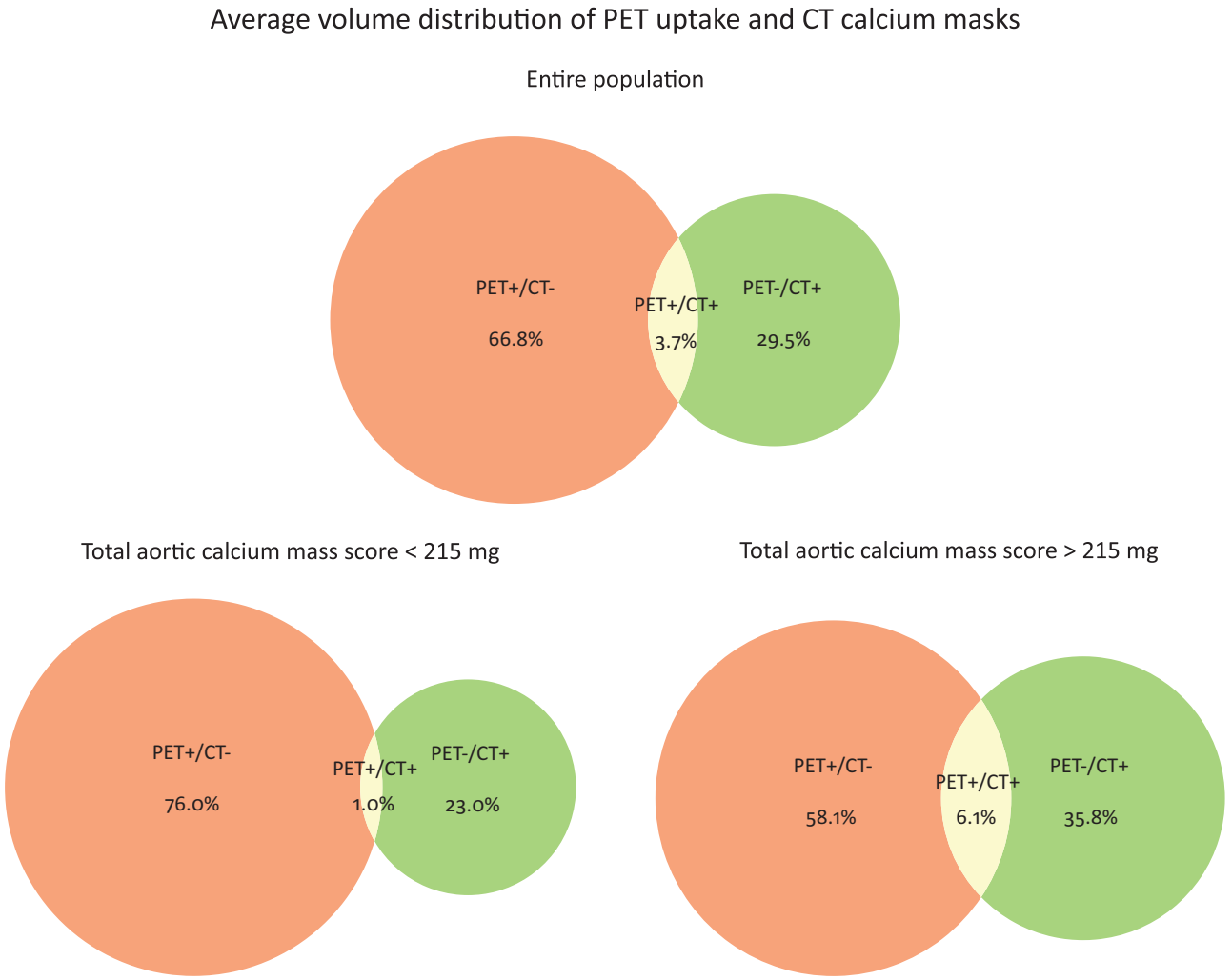

FIGURE 6 3D overlap scores of volume of PET with no overlap of CT (PET+/CT–), volume of CT with no overlap of PET (PET–/CT+), and volumes with both PET and CT (PET+/CT+). The percentages demonstrated are an average of percentage of the volume present in every patient. The upper image demonstrates the average of the three volumes in the entire population. The lower two images demonstrate the average of the three volumes in the group of patients with a calcium mass score lower than 215 mg ($n = 92$; left) and higher than 215 mg ($n = 93$; right).

atherosclerotic plaques and their stability vary across the vascular tree, as the femoral artery is not directly comparable to other arterial compartments.[29] In future research, our method could be used to assess the similarities or differences in atherosclerotic processes between different aortic segments or between different vessels.

Irkle et al. compared Na[^{18}F]F uptake volumes and calcium volumes in carotids of four patients.[16] They found that 95% of the volumes was PET+/CT-, 1% was PET-/CT+, and 4% overlapped, PET+/CT+. In aortas of 186 patients this study demonstrated that 67% of the volumes was PET+/CT-, 29% was PET-/CT+, and again about 4% overlapped, PET+/CT+. The difference between our study and Irkle's et al. may be attributed to variations in population or thresholds used. However, the overlapping percentage was similar.

It should be mentioned that the validity of previous PET studies (in general as well as) looking into individual plaques have been questioned, due to technical limitations of PET.[30] Concerns have been raised regarding the comparison of uptake within and outside calcium masks. It has been debated whether the CT-/PET+ areas just adjacent to CT+ areas might be due to physiological processes or spill-over artifacts, because of the lower resolution of a PET scanner compared with a CT system and because of motion.[31,32] Also, Gaussian smoothing, recommended by the EARL guidelines, smooths out uptake even more. In our study we do see higher TBR values outside the masks for all mass scores and thus various sizes, although not statistically significant for 50+ mg per slice calcifications. Moreover, only a small percentage of calcium mask volumes and Na[^{18}F]F hotspot volumes overlapped.

Due to these limitations of PET, our results must be interpreted with caution. However, the abovementioned results do correspond to the studies demonstrating high specific uptake for the surface of calcifications.[16,31] Recent and upcoming technical advances improved and will improve the resolution of PET systems. The adoption of silicon photomultiplier (SiPM)-based detectors has improved coincidence timing resolution down to about 200 ps, resulting in improved spatial resolution of about 3 mm, and is expected to improve even more.[33] Efforts have been made to optimize the quantification and reproducibility of Na[18F]F PET in atherosclerotic plaque.[34] Electrocardiogram gating can reduce the influence of motion, and partial volume correction algorithms can improve the accuracy of lesion quantification.[35] The revolutionary increase in sensitivity and anatomical coverage of the long-axial field-of-view PET systems give the opportunity to investigate the match/mismatch between Na[18F]F uptake and CT macrocalcifications even more detailed statically and dynamically.[36] Using dynamic parametric imaging on these systems might open up a new application to visualize and quantify smaller and vulnerable plaques.[37] This should be carefully assessed PET in combination with magnetic resonance imaging could evaluate the content of plaque and the degree of plaque activity simultaneously.[38]

To the best of our knowledge, this is the first study to utilise automated patient-specific thresholds for Na[18F]F uptake on PET and compare it directly with calcium masks on CT. Extensive segmentations of entire vessels have been done in earlier studies as well as delineation of hotspots and calcium masks in which SUV or TBR values have been measured. The manual delineation of hotpots is precarious as manual delineation is prone to variability and visual hotspots are dependent on set thresholds or window/level settings. Patient-specific thresholds like the adapted 50% SUV_{peak}—well validated for tumor delineation[25]—minimize differences from normal variation between patients, for example, renal clearance.

Moreover, no previous study visualized calcium distribution and Na[18F]F uptake distribution in a population image. We primarily observed significant calcium accumulation in the inferior abdominal aorta, the inferior aortic arch, and locations corresponding to aortic branches. This is consistent with regions characterized by altered blood flow and low wall shear stress.[39–43] Intriguingly, Na[18F]F exhibited similar behavior, suggesting its potential as a method to assess active atherosclerotic disease states in different arterial beds and to provide important prognostic information beyond conventional methods.[44] This application may become a new clinical tool for the future to reduce or even prevent MACE.

Furthermore, individuals under 65 years old displayed fewer calcifications and less Na[18F]F uptake compared to those above 65 years. Minimal differences were observed between males and females, except for the location of the first aortic branches. The reason behind this discrepancy remains unknown and may be due to chance. Interesting areas with high Na[18F]F uptake but minimal calcification, for example, the superior abdominal aorta, were also identified. The age group above 65 years exhibited slightly more Na[18F]F uptake and macrocalcifications. This could indicate active formation of atherosclerosis, but population-wise slower progression or delayed initiation of atherosclerosis due to lower wall shear stress in that area. The exact reason could be investigated in a longitudinal prospective trial. This gives valuable insight in the behavior of Na[18F]F uptake in the aorta on the population level. Due to the technical limitations of PET discussed before, on the patient level, it would be reasonable to investigate the use of Na[18F]F PET/CT as a global assessment of atherosclerotic burden. Especially in smaller vessels, such as the coronary arteries, it is difficult to evaluate the uptake per lesion. With automated full organ segmentations, this would be possible, and was recently evaluated by Saboury et al. with the Alavi-Carlsen calcification score.[45] It should be investigated whether a similar analysis in the aorta, taking into account spill-over from the vertebra, would be of added clinical value. Cardiac and respiratory motion correction will, however, be key in this process to accurately quantify Na[18F]F uptake.[30]

This study has limitations. First, this was a single center, single manufacturer study. However, our results align with studies conducted at other centers with different scanners. Second, multiple PET systems with different resolutions have been used, which may have slightly impacted the results. However, using EARL recontructions for all scans minimized this effect.[22] Third, delineation of the aortas have been done manually by one observer, which is prone to variability. To get more standardized aortic wall results, automated segmentation models should be used in future studies. Fourth, registration of the aortas may cause deformation of calcium and hotspot masks. However, multiple methods have minimised this effect. The registration was done per segment instead of on the entire aorta. The patient with the median aortic volume was used as the fixed image, to minimise the differences in size between patients. By plotting the results onto a 2D surface mesh, these deformations are blurred out.

To conclude, this study demonstrated that in a population of 186 retrospective clinical Na[18F]F-PET/CT scans Na[18F]F uptake in the aorta behaves similarly to macrocalcification detectable on CT. Na[18F]F uptake values moderately correlated to calcium mass scores. This was shown in a unique population image, which can be viewed in a video online. Notably, higher uptake values were observed outside macrocalcification masks instead of inside the macrocalcification masks. These results correspond with the hypothesis that Na[18F]F

binds to the surface of calcifications. This could be of special interest for unstable plaques.

ACKNOWLEDGMENT

Funded by Siemens Medical Solutions USA (Siemens Healthineers USA).

CONFLICT OF INTEREST STATEMENT

Gijs D. van Praagh: This study was in part supported by an unconditional grant from PUSH: a collaboration between Siemens Healthineers and the University Medical Center Groningen. The sponsor had no institutional role in the conceptualization, writing, or publication of the article. M. E. J. Davidse: The author has no conflicts of interest to disclose. J. M. Wolterink: The author has no conflicts of interest to disclose. R. H. J. A. Slart: This study was in part supported by an unconditional grant from PUSH: a collaboration between Siemens Healthineers and the University Medical Center Groningen. The sponsor had no institutional role in the conceptualization, writing, or publication of the article.

DATA AVAILABILITY STATEMENT

The data that support the findings of this study are available from the corresponding author upon reasonable request. The data are not publicly available due to privacy or ethical restrictions.

REFERENCES

1. Roth GA, Abate D, Abate KH, et al. Global, regional, and national age-sex-specific mortality for 282 causes of death in 195 countries and territories, 1980–2017: a systematic analysis for the Global Burden of Disease Study 2017. *Lancet*. 2018;392(10159):1736-1788. doi:10.1016/S0140-6736(18)32203-7
2. Ahmed HM, Blaha MJ, Nasir K, et al. Low-risk lifestyle, coronary calcium, cardiovascular events, and mortality: results from MESA. *Am J Epidemiol*. 2013;178(1):12-21. doi:10.1093/aje/kws453
3. Blaha MJ, Cainzos-Achirica M, Greenland P, et al. Role of coronary artery calcium score of zero and other negative risk markers for cardiovascular disease: the multi-ethnic study of atherosclerosis (MESA). *Circulation*. 2016;133(9):849-858. doi:10.1161/CIRCULATIONAHA.115.018524
4. Agatston AS, Janowitz WR, Hildner FJ, Zusmer NR, Viamonte M, Detrano R. Quantification of coronary artery calcium using ultrafast computed tomography. *J Am Coll Cardiol*. 1990;15(4):827-832. doi:10.1016/0735-1097(90)90282-T
5. Kelly-Arnold A, Maldonado N, Laudier D, Aikawa E, Cardoso L, Weinbaum S. Revised microcalcification hypothesis for fibrous cap rupture in human coronary arteries. *Proc Natl Acad Sci*. 2013;110(26):10741-10746. doi:10.1073/pnas.1308814110
6. Richardson PD, Davies MJ, Born GV. Influence of plaque configuration and stress distribution on fissuring of coronary atherosclerotic plaques. *Lancet Lond Engl*. 1989;2(8669):941-944. doi:10.1016/s0140-6736(89)90953-7
7. Maldonado N, Kelly-Arnold A, Vengrenyuk Y, et al. A mechanistic analysis of the role of microcalcifications in atherosclerotic plaque stability: potential implications for plaque rupture. *Am J Physiol—Heart Circ Physiol*. 2012;303(5):H619-H628. doi:10.1152/ajpheart.00036.2012
8. Vengrenyuk Y, Carlier S, Xanthos S, et al. A hypothesis for vulnerable plaque rupture due to stress-induced debonding around cellular microcalcifications in thin fibrous caps. *Proc Natl Acad Sci USA*. 2006;103(40):14678-14683. doi:10.1073/pnas.0606310103
9. Criqui MH, Denenberg JO, Ix JH, et al. Calcium density of coronary artery plaque and risk of incident cardiovascular events. *JAMA—J Am Med Assoc*. 2014;311(3):271-278. doi:10.1001/jama.2013.282535
10. Callister TQ, Cooil B, Raya SP, Lippolis NJ, Russo DJ, Raggi P. Coronary artery disease: improved reproducibility of calcium scoring with an electron-beam CT volumetric method. *Radiology*. 1998;208(3):807-814. doi:10.1148/radiology.208.3.9722864
11. McCollough CH. Computed tomography technology—and dose—in the 21st century. *Health Phys*. 2019;116:157-162. doi:10.1097/HP.0000000000000997
12. Blaha MJ, Mortensen MB, Kianoush S, Tota-Maharaj R, Cainzos-Achirica M. Coronary artery calcium scoring: is it time for a change in methodology? *JACC Cardiovasc Imaging*. 2017;10(8):923-937. doi:10.1016/j.jcmg.2017.05.007
13. Willemink MJ, van der Werf NR, Nieman K, Greuter MJW, Koweek LM, Fleischmann D. Coronary artery calcium: a technical argument for a new scoring method. *J Cardiovasc Comput Tomogr*. 2019;13(6):347-352. doi:10.1016/j.jcct.2018.10.014
14. Sandfort V, Persson M, Pourmorteza A, Noël PB, Fleischmann D, Willemink MJ. Spectral photon-counting CT in cardiovascular imaging. *J Cardiovasc Comput Tomogr*. 2021;15(3):218-225. doi:10.1016/j.jcct.2020.12.005
15. Abedin M, Tintut Y, Demer LL. Vascular calcification: mechanisms and clinical ramifications. *Arterioscler Thromb Vasc Biol*. 2004;24(7):1161-1170. doi:10.1161/01.ATV.0000133194.94939.42
16. Irkle A, Vesey AT, Lewis DY, et al. Identifying active vascular microcalcification by 18F-sodium fluoride positron emission tomography. *Nat Commun*. 2015;6(1):7495. doi:10.1038/ncomms8495
17. Forbang NI, Michos ED, McClelland RL, et al. Greater volume but not higher density of abdominal aortic calcium is associated with increased cardiovascular disease risk: the multi-ethnic study of atherosclerosis (MESA). *Circ Cardiovasc Imaging*. 2016;9(11):e005138. doi:10.1161/CIRCIMAGING.116.005138
18. Han D, Klein E, Friedman J, et al. Prognostic significance of subtle coronary calcification in patients with zero coronary artery calcium score: from the CONFIRM registry. *Atherosclerosis*. 2020;309(June):33-38. doi:10.1016/j.atherosclerosis.2020.07.011
19. Joshi NV, Vesey AT, Williams MC, et al. 18F-fluoride positron emission tomography for identification of ruptured and high-risk coronary atherosclerotic plaques: a prospective clinical trial. *Lancet*. 2014;383(9918):705-713. doi:10.1016/S0140-6736(13)61754-7
20. Dweck MR, Chow MWL, Joshi NV, et al. Coronary arterial 18F-sodium fluoride uptake: a novel marker of plaque biology. *J Am Coll Cardiol*. 2012;59(17):1539-1548. doi:10.1016/j.jacc.2011.12.037
21. Czernin J, Satyamurthy N, Schiepers C. Molecular mechanisms of bone 18F-NaF deposition. *J Nucl Med*. 2010;51(12):1826-1829. doi:10.2967/jnumed.110.077933
22. Beheshti M, Mottaghy FM, Paycha F, et al. ^{18}F-NaF PET/CT: eANM procedure guidelines for bone imaging. *Eur J Nucl Med Mol Imaging*. 2015;42(11):1767-1777. doi:10.1007/s00259-015-3138-y
23. Lessmann N, van Ginneken B, de Jong PA, Išgum I. Iterative fully convolutional neural networks for automatic vertebra segmentation and identification. *Med Image Anal*. 2019;53:142-155. doi:10.1016/j.media.2019.02.005
24. Raggi P, Callister TQ, Cooil B. Calcium scoring of the coronary artery by electron beam CT. *Am J Roentgenol*. 2002;178(2):497-502. doi:10.2214/ajr.178.2.1780497
25. Frings V, de Langen AJ, Smit EF, et al. Repeatability of metabolically active volume measurements with 18F-FDG and 18F-FLT

PET in non-small cell lung cancer. *J Nucl Med*. 2010;51(12):1870-1877. doi:10.2967/jnumed.110.077255
26. Marstal K, Berendsen F, Staring M, Klein S. SimpleElastix: a user-friendly, multi-lingual library for medical image registration. In: *2016 IEEE Conference on Computer Vision and Pattern Recognition Workshops (CVPRW)*. IEEE; 2016:574-582. doi:10.1109/CVPRW.2016.78
27. McKenney-Drake ML, Moghbel MC, Paydary K, et al. ^{18}F-NaF and ^{18}F-FDG as molecular probes in the evaluation of atherosclerosis. *Eur J Nucl Med Mol Imaging*. 2018;45(12):2190-2200. doi:10.1007/s00259-018-4078-0
28. den Harder AM, Wolterink JM, Bartstra JW, et al. Vascular uptake on ^{18}F-sodium fluoride positron emission tomography: precursor of vascular calcification? *J Nucl Cardiol*. 2021;28(5):2244-2254. doi:10.1007/s12350-020-02031-5
29. Banerjee S. Superficial femoral artery is not left anterior descending artery. *Circulation*. 2016;134(13):901-903. doi:10.1161/CIRCULATIONAHA.116.023690
30. Alavi A, Werner TJ, Høilund-Carlsen PF. What can be and what cannot be accomplished with PET to detect and characterize atherosclerotic plaques. *J Nucl Cardiol*. 2018;25(6):2012-2015. doi:10.1007/s12350-017-0977-x
31. Creager MD, Hohl T, Hutcheson JD, et al. ^{18}F-Fluoride signal amplification identifies microcalcifications associated with atherosclerotic plaque instability in positron emission tomography/computed tomography images. *Circ Cardiovasc Imaging*. 2019;12(1):e007835. doi:10.1161/CIRCIMAGING.118.007835
32. Demer LL, Tintut Y, Nguyen KL, Hsiai T, Lee JT. Rigor and reproducibility in analysis of vascular calcification. *Circ Res*. 2017;120(8):1240-1242. doi:10.1161/CIRCRESAHA.116.310326
33. Hutton BF, Erlandsson K, Thielemans K. Advances in clinical molecular imaging instrumentation. *Clin Transl Imaging*. 2018;6(1):31-45. doi:10.1007/s40336-018-0264-0
34. Moss AJ, Doris MK, Andrews JPM, et al. Molecular coronary plaque imaging using ^{18}F-Fluoride. *Circ Cardiovasc Imaging*. 2019;12(8):e008574. doi:10.1161/CIRCIMAGING.118.008574
35. Cal-Gonzalez J, Li X, Heber D, et al. Partial volume correction for improved PET quantification in 18F-NaF imaging of atherosclerotic plaques. *J Nucl Cardiol*. 2018;25(5):1742-1756. doi:10.1007/s12350-017-0778-2
36. Slart R, Tsoumpas C, Glaudemans A, et al. Long axial field of view PET scanners: a road map to implementation and new possibilities. *Eur J Nucl Med Mol Imaging*. 2021;48(13):4236-4245. doi:10.1007/s00259-021-05461-6
37. Rahmim A, Lodge MA, Karakatsanis NA, et al. Dynamic whole-body PET imaging: principles, potentials and applications. *Eur J Nucl Med Mol Imaging*. 2019;46(2):501-518. doi:10.1007/s00259-018-4153-6
38. Naeger DM, Behr SC. PET/MR imaging: current and future applications for cardiovascular disease. *Magn Reson Imaging Clin N Am*. 2015;23(1):95-103. doi:10.1016/j.mric.2014.09.006
39. Gibson CM, Diaz L, Kandarpa K, et al. Relation of vessel wall shear stress to atherosclerosis progression in human coronary arteries. *Arterioscler Thromb J Vasc Biol*. 1993;13(2):310-315. doi:10.1161/01.ATV.13.2.310
40. Soulis JV, Fytanidis DK, Papaioannou VC, Giannoglou GD. Wall shear stress on LDL accumulation in human RCAs. *Med Eng Phys*. 2010;32(8):867-877. doi:10.1016/j.medengphy.2010.05.011
41. Sun Y, Zhang B, Xia L. Effect of low wall shear stress on the morphology of endothelial cells and its evaluation indicators. *Comput Methods Programs Biomed*. 2021;208:106082. doi:10.1016/j.cmpb.2021.106082
42. Desai MY, Cremer PC, Schoenhagen P. Thoracic aortic calcification: diagnostic, prognostic, and management considerations. *JACC Cardiovasc Imaging*. 2018;11(7):1012-1026. doi:10.1016/j.jcmg.2018.03.023
43. Chuang ML, Leslie RW, Massaro JM, et al. Distribution of abdominal aortic calcium by computed tomography: impact of analysis method on quantitative calcium score. *Acad Radiol*. 2013;20(11):1422-1428. doi:10.1016/j.acra.2013.08.008
44. Forsythe RO, Dweck MR, McBride OMB, et al. 18F-sodium fluoride uptake in abdominal aortic aneurysms: the SoFIA3 study. *J Am Coll Cardiol*. 2018;71(5):513-523. doi:10.1016/j.jacc.2017.11.053
45. Saboury B, Edenbrandt L, Piri R, et al. Alavi–Carlsen Calcification Score (ACCS): a simple measure of global cardiac atherosclerosis burden. *Diagnostics*. 2021;11(8):1421. doi:10.3390/diagnostics11081421

SUPPORTING INFORMATION

Additional supporting information can be found online in the Supporting Information section at the end of this article.

How to cite this article: van Praagh GD, Davidse MEJ, Wolterink JM, Slart R. Quantitative analysis of aortic Na[^{18}F]F uptake in macrocalcifications and microcalcifications in PET/CT scans. *Med Phys*. 2023;1-10. https://doi.org/10.1002/mp.16787